

LCLS-II HXR and SXR FEL Estimates for the Cu Linac Beam

Heinz-Dieter Nuhn^a

^aSLAC National Accelerator Laboratory, Stanford University, CA 94309-0210, USA

Abstract

Operation of the LCLS-II undulator lines is scheduled to start in 2020 with electron beams from the existing Cu linac running with up to 120 bunches per second shared between the hard x-ray (HXR) and soft x-ray (SXR) beamlines. This document attempts to predict achievable per-pulse x-ray beam intensities for running these beamlines in SASE mode with Cu linac electron beams.

Keywords: SASE, Undulator, FEL

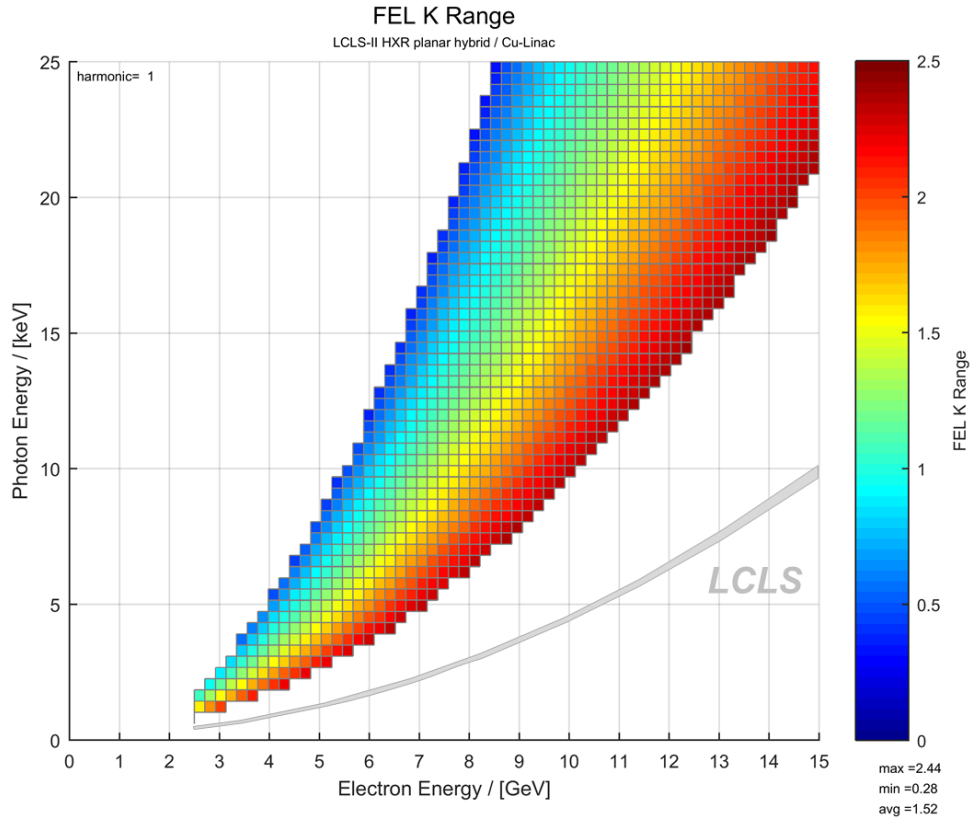
1. INTRODUCTION

The LCLS Free Electron Laser (FEL) has been producing high brightness x-ray pulses with a single undulator beamline (33 undulator segments) from electron bunches produced by a photocathode RF gun and accelerated by the last 3rd of the SLAC linac. This undulator beamline is currently being replaced by an HXR beamline in its old location and an SXR beamline parallel to it as part of the LCLS-II construction project at SLAC. The project provides a transport line from the last 3rd of the SLAC Cu linac to the HXR beamline. Currently, an additional transport line connecting the Cu linac to the SXR beamline is being built, with off-project funding. A beam distribution magnet will send the up to 120 electron bunches per second to one of the undulator beamlines or a dump. When operational, the two undulator beamlines will be run at individual bunch repetition rates that add up to 120 Hz or less. Table 1 shows a comparison of basic parameters of the old and new systems.

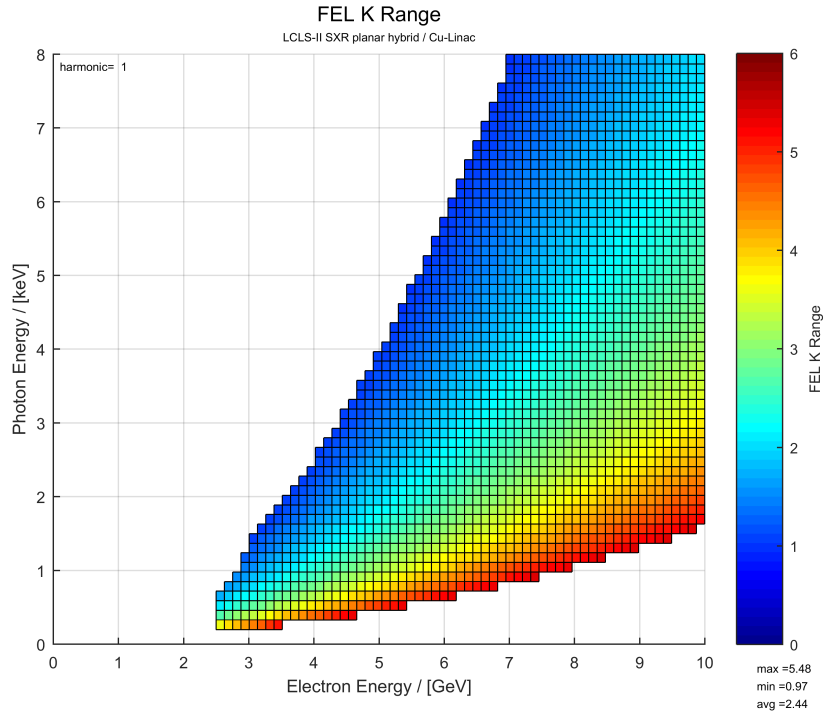
Table 1: Parameter Comparison between the old LCLS and the new LCLS-II undulator beamline when operated from the Cu linac.

Parameter	LCLS	HXR	SXR	Unit
Number of Undulator Segments	33 (31)	32	21	
Undulator Period Length	30	26	39	mm
Segment Length	3.4	3.4	3.4	m
Operational Undulator Gap Range	6.781 — 6.887	7.2 — 20	7.2 — 22	mm
Operational Undulator K Range	3.51 — 3.45	2.44 — \approx 0.5	5.48 — \approx 1.0	
Operational Electron Energy Range	2.5 — <17.0	2.5 — <17.0	2.5 — 10.0	GeV
Maximum Operational Photon Energy Range	0.28 — <13.0	0.2 — 25.0	0.2 — 8.0	keV

Figure 1 illustrates how the K values need to be set to reach the operating combinations of electron energy and photon energy. In this and the following figures of the same kind, the colored squares indicate combination of electron energy and photon energy where FEL operation is possible. (For range comparison, the old LCLS range is indicated in gray color). The color code is explained on the right-hand-side of each figure. Figure 2 presents the undulator gap settings corresponding to the K values of Figure 1. As can be seen in subplot (a) of Figure 2, with the HXR beamline, the maximum nominal operational photon energy of 25 keV can be reached at gap values close to the minimum gap (corresponding to the highest K value). Increasing the gap will allow to operate at higher photon energies at a given electron energy. The achievable FEL x-ray intensity is highest at the smallest gap (i.e., highest K) values. The intensity becomes insignificant towards the upper end of the operational gap range, shown in Table 1. In addition, the Cu-linac is capable of reaching higher electron energies than the nominal ranges shown. The maximum reachable electron energy of the Cu linac is between 16 GeV and 17 GeV, limited by klystron power. This extra electron energy range can be used to increase the range of available photon energies even further.

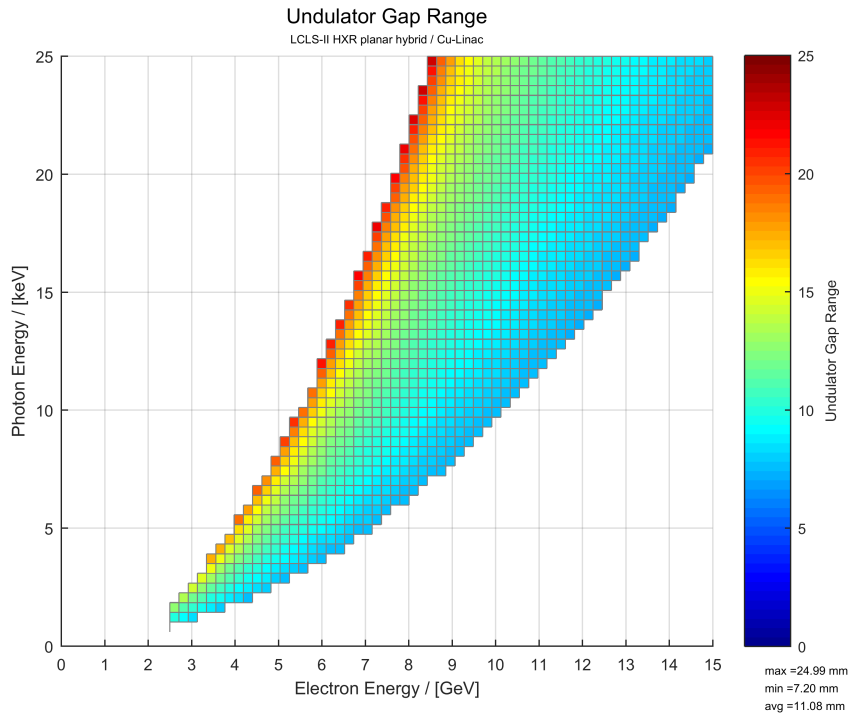


(a) HXR with Cu Linac

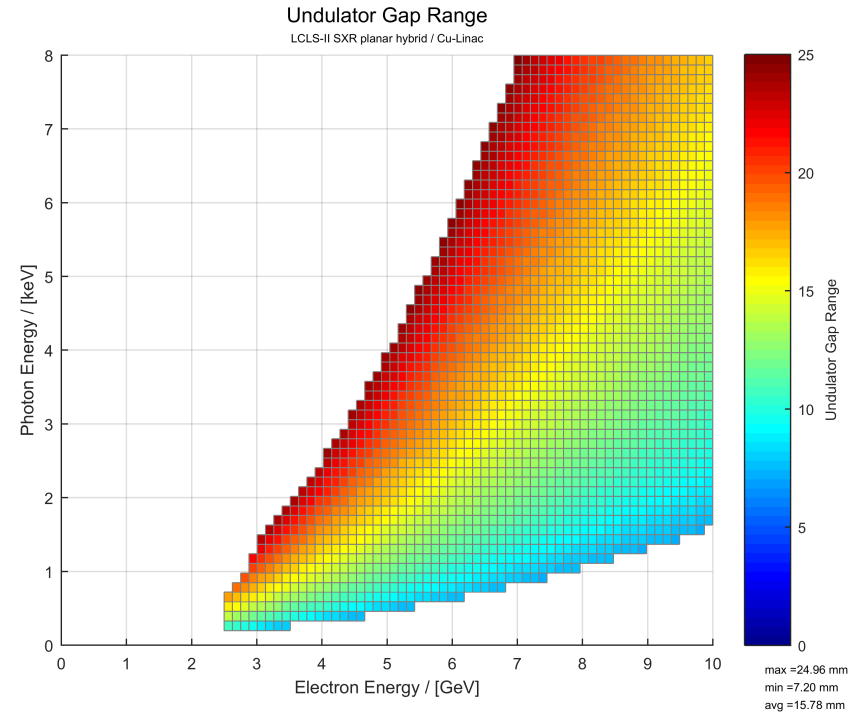


(b) SXR with Cu Linac

Figure 1: K values required to control the operational range for the HXR and SXR beamlines line as function of electron and photon energies for Cu-linac.



(a) HXR with Cu Linac



(b) SXR with Cu Linac

Figure 2: Undulator gap values required to control the operational range for the HXR and SXR beamlines line as function of electron and photon energies for Cu-linac.

2. FEL SASE INTENSITY ESTIMATES

2.1. SXR Beamlne

In order to predict FEL pulse intensities in SASE (Self Amplified Spontaneous Emission) mode for the FEL beamlines, we have developed a model based on the well known formula published by Ming Xie [1] adjusted with empirical scaling, including support for post-saturation taper, to match LCLS performance. In the past, we used this model also to predict performance for the LCLS-II HXR and SXR beamlines when operated with the copper linac. For this paper we changed strategy by using LCLS-II start-to-end simulation results for the SXR beamline [2] as matching target instead of LCLS performance and also upgraded the post-saturation taper support to reflect the expected increased taper efficiency for the LCLS-II undulator systems because of the presence of phase shifters.

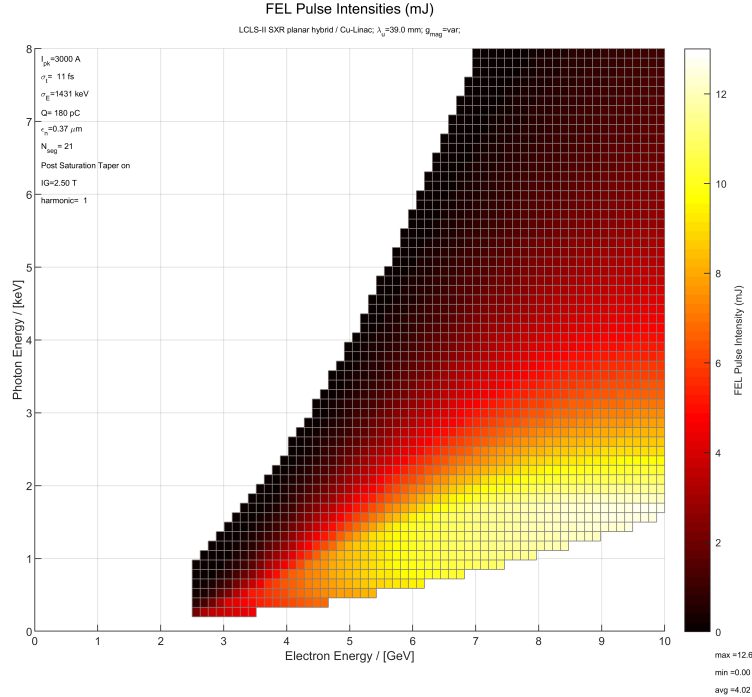


Figure 3: FEL SASE intensity predictions for the LCLS-II SXR line matching start-to-end FEL simulations [2] at (10 GeV, 1.5 keV) and (10 GeV, 5.0 keV).

Figure 3 shows the LCLS-II SXR beamline SASE FEL intensity predictions using parameters of FEL start-to-end simulations that served as matching target.

The prediction of the total pulse intensity for a given electron energy/photon energy operating point depends on a number of key parameters, predominantly electron beam slice emittance, energy spread, peak current, bunch charge, and quadrupole focusing strength. Secondary parameters include electron beam projected emittance due to position chirp and trajectory. The predictions made in this paper assume a chirp-free beam with no trajectory oscillations. The primary parameters are dependent on each other and on other parameters and can vary over a significant range:

electron beam slice emittance depends on cathode quality, laser beam spot size, bunch charge and beam transport.

energy spread is determined by the laser heater amplitude and the bunch compression factor (or peak current).

peak current depends on bunch charge and bunch length.

bunch charge has values between 20 pC and 250 pC.

Analyses of the effect of these parameter ranges on predicted x-ray intensity show that while the distribution of intensities, in the colored area in Figure 3, varies as these key parameters change values, the predicted FEL intensities amplitudes stay below 1.3 times the values shown in the figure.

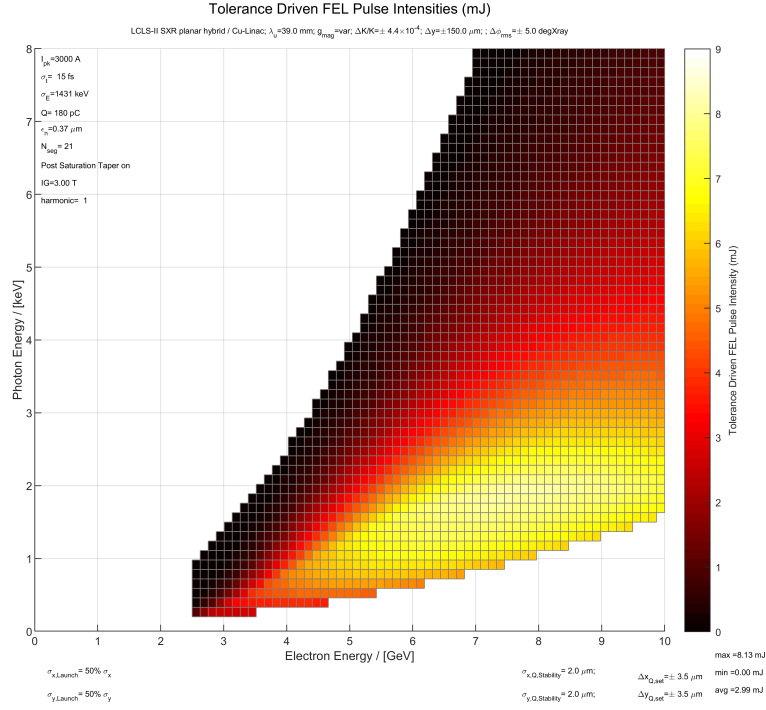


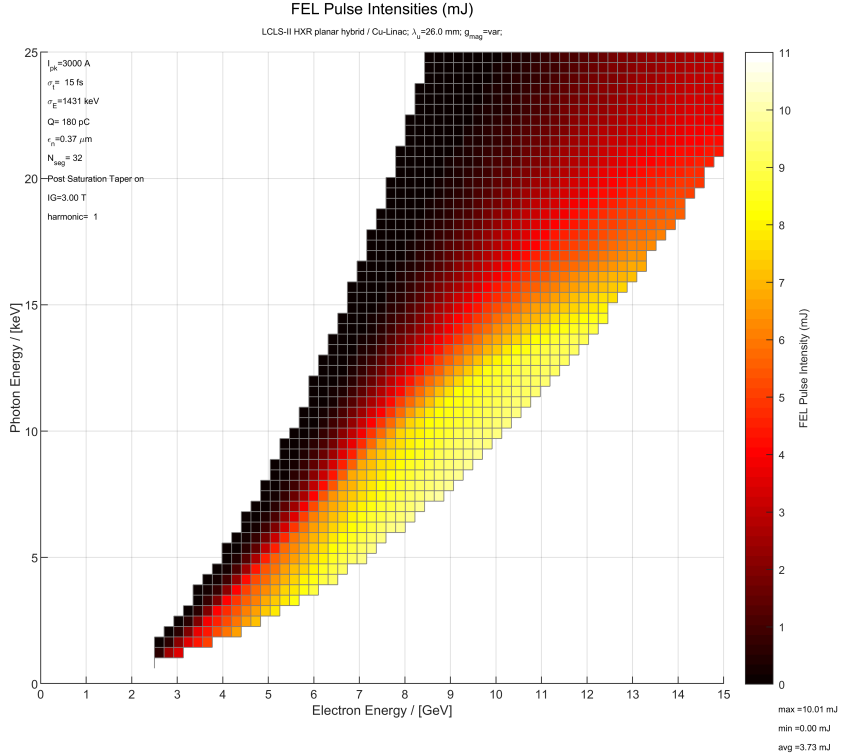
Figure 4: FEL intensity predictions for the LCLS-II SXR line including performance reductions based on undulator system tolerances.

The results shown in Figure 3 were obtained under the assumption of a perfect undulator system. In reality, tolerances have been established for a number of undulator system parameters. FEL performance can be reduced depending on the level to which the individual tolerance ranges have been used.

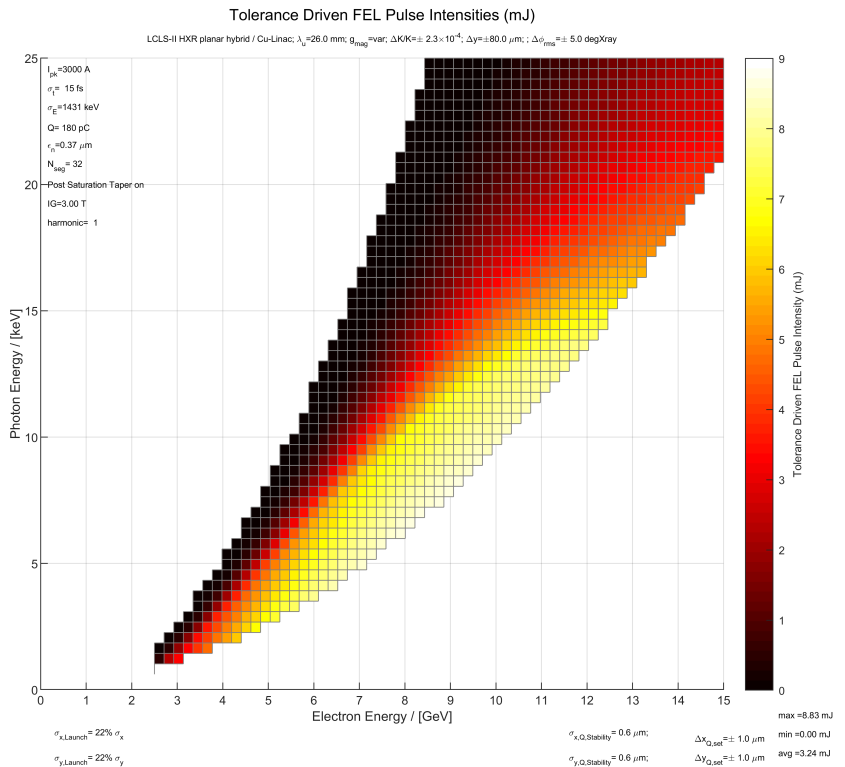
An estimate of the intensity reduction when applying the full tolerance effects to the values shown in Figure 3 is shown in Figure 4. A list of intensity predictions is given in Table 2 in the Appendix.

2.2. HXR Beamlne

Applying the same algorithm to the prediction of HXR FEL SASE performance results in the values shown in Figure 5a is shown in Figure 5b. A list of intensity predictions is given in Table 3 in the Appendix.



(a) HXR with Cu Linac



(b) HXR with Cu Linac including tolerance reductions

Figure 5: Intensity predictions for the LCLS-II HXR beamline with electrons beam from the Cu-linac.

2.3. Summary

This paper attempts to provide estimates for the per-bunch x-ray beam intensity levels that might be achieved in the LCLS-II SXR and HXR beamlines when operated with beam from the Cu linac in SASE mode.

Appendix

Table 2: SXR Undulator Beamline x-ray intensity predictions.

E_{ph} (keV)	tol E_{xray} (mJ)	no tol E_{xray} (mJ)	max E_{xray} (mJ)	Θ_{rms} (μ rad)	z_{src} (m)	E_e (GeV)
0.20	2.7	5.0	6.5	23.93	-44.1	3.52
0.33	3.9	7.2	9.3	16.56	-44.9	4.66
0.46	4.7	8.5	11.1	12.68	-43.8	5.42
0.59	5.4	9.6	12.5	10.35	-42.7	6.19
0.72	6.0	10.4	13.6	8.77	-41.5	6.82
0.85	6.4	11.1	14.4	7.63	-40.3	7.46
0.98	6.8	11.6	15.0	6.76	-39.2	7.97
1.11	7.1	11.9	15.5	6.09	-38.1	8.47
1.24	7.4	12.2	15.9	5.54	-37.0	8.98
1.37	7.6	12.4	16.2	5.09	-36.0	9.49
1.50	7.8	12.6	16.4	4.71	-35.1	9.87
1.63	7.9	12.7	16.5	4.38	-34.3	10.00
1.76	8.0	12.8	16.6	4.11	-33.6	10.00
1.89	8.1	12.8	16.7	3.86	-32.9	10.00
2.02	7.9	12.3	15.9	3.65	-32.4	9.49
2.15	7.5	11.6	15.1	3.46	-31.7	9.62
2.28	7.1	11.0	14.2	3.29	-31.1	9.62
2.41	6.8	10.4	13.5	3.14	-30.5	9.75
2.54	6.5	9.8	12.8	3.01	-29.9	9.87
2.67	6.2	9.3	12.1	2.88	-29.3	10.00
2.80	5.9	8.9	11.5	2.77	-28.7	10.00
2.93	5.6	8.4	11.0	2.66	-28.2	10.00
3.06	5.3	8.0	10.4	2.57	-27.7	10.00
3.19	5.1	7.7	9.9	2.48	-27.2	10.00
3.32	4.9	7.3	9.5	2.39	-26.7	10.00
3.45	4.7	7.0	9.0	2.32	-26.2	10.00
3.58	4.4	6.6	8.6	2.25	-25.7	10.00
3.71	4.3	6.3	8.2	2.18	-25.2	10.00
3.84	4.1	6.0	7.9	2.12	-24.7	10.00
3.97	3.9	5.8	7.5	2.06	-24.2	10.00
4.10	3.7	5.5	7.2	2.00	-23.8	10.00
4.23	3.6	5.3	6.8	1.95	-23.3	10.00
4.36	3.4	5.0	6.5	1.90	-22.9	10.00

4.49	3.3	4.8	6.3	1.85	-22.4	10.00
4.62	3.1	4.6	6.0	1.81	-22.0	10.00
4.75	3.0	4.4	5.7	1.77	-21.5	10.00
4.88	2.9	4.2	5.5	1.73	-21.1	10.00
5.01	2.7	4.0	5.2	1.69	-20.6	10.00
5.14	2.6	3.9	5.0	1.65	-20.2	10.00
5.27	2.5	3.7	4.8	1.62	-19.7	10.00
5.40	2.4	3.5	4.6	1.59	-19.3	10.00
5.53	2.3	3.4	4.4	1.55	-18.9	10.00
5.66	2.2	3.2	4.2	1.52	-18.4	10.00
5.79	2.1	3.1	4.0	1.49	-18.0	10.00
5.92	2.0	3.0	3.9	1.47	-17.5	10.00
6.05	1.9	2.8	3.7	1.44	-17.1	10.00
6.18	1.8	2.7	3.5	1.41	-16.7	10.00
6.31	1.7	2.6	3.4	1.39	-16.2	10.00
6.44	1.6	2.5	3.2	1.37	-15.8	10.00
6.57	1.6	2.4	3.1	1.34	-15.3	10.00
6.70	1.5	2.3	3.0	1.32	-14.9	10.00
6.83	1.4	2.2	2.8	1.30	-14.4	10.00
6.96	1.4	2.1	2.7	1.28	-14.0	10.00
7.09	1.3	2.0	2.6	1.26	-13.5	10.00
7.22	1.2	1.9	2.5	1.24	-13.1	10.00
7.35	1.2	1.8	2.4	1.22	-12.6	10.00
7.48	1.1	1.8	2.3	1.20	-12.1	10.00
7.61	1.1	1.7	2.2	1.18	-11.7	10.00
7.74	1.0	1.6	2.1	1.17	-11.7	10.00
7.87	1.0	1.5	2.0	1.15	-11.8	10.00
8.00	0.9	1.5	1.9	1.13	-12.0	10.00

Table 3: HXR Undulator Beamline x-ray intensity predictions.

E_{ph} (keV)	tol	no tol	max	Θ_{rms} (μ rad)	z_{src} (m)	E_e (GeV)
E_{xray} (mJ)	Θ_{rms} (μ rad)	z_{src} (m)	E_e (GeV)			
1.03	4.0	4.3	5.6	6.33	-56.6	3.14
1.44	5.4	5.8	7.6	5.01	-60.3	3.77
1.85	6.5	7.2	9.3	4.16	-61.9	4.41
2.27	7.1	7.8	10.1	3.54	-61.5	4.83
2.68	7.5	8.3	10.8	3.09	-61.1	5.25
3.09	7.9	8.8	11.4	2.75	-60.7	5.68
3.51	8.3	9.2	11.9	2.48	-60.2	6.10
3.92	8.5	9.5	12.4	2.26	-59.7	6.52

4.33	8.5	9.5	12.4	2.08	-58.8	6.74
4.75	8.7	9.8	12.7	1.93	-58.3	7.16
5.16	8.7	9.8	12.7	1.79	-57.5	7.37
5.57	8.7	9.7	12.7	1.68	-56.7	7.58
5.99	8.8	9.9	12.9	1.58	-56.2	8.01
6.40	8.8	9.9	12.9	1.49	-55.5	8.22
6.81	8.7	9.9	12.8	1.42	-54.8	8.43
7.23	8.8	10.0	13.0	1.35	-54.3	8.86
7.64	8.8	10.0	12.9	1.29	-53.6	9.07
8.05	8.7	9.9	12.9	1.23	-52.9	9.28
8.47	8.6	9.9	12.8	1.18	-52.3	9.49
8.88	8.6	9.8	12.7	1.13	-51.7	9.70
9.29	8.5	9.8	12.7	1.09	-51.1	9.92
9.71	8.5	9.7	12.6	1.05	-50.5	10.13
10.12	8.4	9.6	12.5	1.01	-49.9	10.34
10.53	8.3	9.6	12.5	0.98	-49.3	10.55
10.95	8.2	9.5	12.4	0.94	-48.8	10.76
11.36	8.2	9.5	12.3	0.91	-48.2	10.97
11.77	8.1	9.4	12.2	0.89	-47.7	11.19
12.19	8.0	9.4	12.2	0.86	-47.1	11.40
12.60	8.0	9.3	12.1	0.84	-46.6	11.61
13.01	7.9	9.2	12.0	0.81	-46.1	11.82
13.43	7.8	9.2	11.9	0.79	-45.6	12.03
13.84	7.7	9.0	11.7	0.77	-45.1	12.25
14.25	7.3	8.6	11.2	0.75	-44.6	12.46
14.67	6.9	8.2	10.6	0.73	-44.0	12.46
15.08	6.6	7.8	10.2	0.72	-43.5	12.67
15.49	6.3	7.5	9.8	0.70	-43.0	12.88
15.91	6.1	7.2	9.4	0.68	-42.5	13.09
16.32	5.8	6.9	9.0	0.67	-42.1	13.30
16.73	5.5	6.6	8.6	0.65	-41.5	13.30
17.15	5.3	6.3	8.3	0.64	-41.0	13.52
17.56	5.1	6.1	7.9	0.63	-40.6	13.73
17.97	4.9	5.9	7.6	0.61	-40.2	13.94
18.39	4.7	5.7	7.4	0.60	-39.7	14.15
18.80	4.5	5.4	7.0	0.59	-39.2	14.15
19.21	4.3	5.2	6.8	0.58	-38.8	14.36
19.63	4.1	5.0	6.5	0.57	-38.3	14.58
20.04	3.9	4.8	6.2	0.56	-37.8	14.58
20.45	3.8	4.6	6.0	0.55	-37.4	14.79
20.87	3.7	4.5	5.8	0.54	-37.0	15.00

21.28	3.5	4.3	5.5	0.53	-36.5	15.00
21.69	3.3	4.1	5.3	0.52	-35.9	15.00
22.11	3.2	3.9	5.1	0.51	-35.4	15.00
22.52	3.0	3.7	4.8	0.51	-34.9	15.00
22.93	2.9	3.5	4.6	0.50	-34.3	15.00
23.35	2.8	3.4	4.4	0.49	-33.8	15.00
23.76	2.6	3.2	4.2	0.48	-33.2	15.00
24.17	2.5	3.1	4.0	0.48	-32.6	15.00
24.59	2.4	2.9	3.8	0.47	-32.1	15.00
25.00	2.3	2.8	3.6	0.46	-31.5	15.00

References

- [1] M. Xie, “Design Optimization for an X-ray Free Electron Laser Driven by SLAC Linac,” *LBL Preprint No-36038*, p. 3, 1995.
- [2] G. Marcus, Y. Ding, 2016. Private Communication.